TURBOMACHINERY & PUMP SYMPOSIA | HOUSTON, TX
DECEMBER 14-16, 2021
SHORT COURSES: DECEMBER 13, 2021

AN EFFECTIVE METHOD TO SEPARATE THE FORWARD AND BACKWARD NATURAL FREQUENCIES IN TURBOMACHINERY VIBRATION TEST MEASUREMENTS

Tingcheng Wu
Senior Rotordynamic R&D Engineer
Siemens Energy
Olean, New York, USA

Martin D. Maier
Principal Rotor Dynamic Analysis Engineer
Siemens Energy
Olean, New York, USA

Dr. Tingcheng Wu is a senior Rotordynamic R&D Engineer at Siemens Energy. His duty includes the torsional and lateral rotor dynamic analysis, bearing and seal design, and machinery vibration analysis. In addition, he has developed several automation tools for the company's in-house rotordynamic analysis. He received his B.S. in mechanical engineering from Nanjing University of Science and Technology in 2011. After that, he worked as a mechanical engineer at China Aerospace Research Academy. He received his M.S. in mechanical engineering from the University of Houston in 2014 and his Ph.D. degree from the Turbomachinery Laboratory at Texas A&M University in 2019. His interest includes numerical and experimental analysis of turbomachine rotordynamics and vibration issues. He has published 19 technical papers and reports in international conferences and journals. Dr. Wu is a session chair for the Structures and Dynamics section of ASME IGTI Turbo Expo Conference, and he also serves as the Technical Editor of STLE Tribology and Lubrication Technology.

Martin D. Maier is a Principal Rotor Dynamic Analysis Engineer at Siemens Energy. He has 44 years of experience with Dresser-Rand in torsional and lateral rotor dynamic analysis, coupling, bearing/seal design, and machinery vibration analysis related to product development and production support. His experience includes program automation, engineering standards development and vibration troubleshooting. Mr. Maier received a B.S. degree in Physics in 1977 and a B.S degree in Mechanical Engineering in 1990, both from the Rochester Institute of Technology. He is a licensed Professional Engineer in New York State, since 1991, and is a member of the Vibration Institute with a Level IV, Machinery Analyst Certification. He has received several U.S. patents in bearing, seal, and aerodynamic design.

ABSTRACT

As speed and power density increase, validation of analytical prediction with actual test data plays an important role to ensure avoidance of critical speeds in high-speed turbomachinery and a reliable design. For a typical centrifugal compressor, the location of its second critical speed usually limits the maximum speed it can operate. Due to the gyroscopic effect, the difference between some forward and backward natural frequencies increases with the rotating speed. To identify the two different natural frequencies experimentally, common engineering practice requires excitations with forward and backward rotating excitations, separately.

This paper includes two case studies to benchmark the method. The first case study is a comparison between theoretical predictions. The second case study presents a comparison between predicted and measured results from a 21,700 HP (16 MW) full-load, full-pressure test. This test was conducted using a magnetitic bearing exciter applied to a 6 stage back-to-back centrifugal compressor designed for natural gas processing. The example provided will show identification and extraction of the natural frequencies below MCOS, excited sub-synchronously and above MCOS, excited super-synchronously. Additionally, based on the Bently Nevada full spectrum plot theory, the paper presents an effective approach to identifying the forward and backward natural frequencies from a single planar excitation, reducing 50% of the test time and cost. The theory and characteristic equation will be shown along with the comparisons with both simulated and test results which serve to validate the accuracy of this method.

INTRODUCTION

For a typical centrifugal compressor, the second critical speed usually plays an important role in limiting the compressor's maximum operating speed. The API 617 standard requires a separation margin for each critical speed to ensure the safe operation [1]. Therefore, accurate identification of the critical speeds is vital in centrifugal compressor design and test. In engineering practice, unbalance response analysis is used to identify the compressor first and second critical speeds [2-4].

The gyroscopic effect in the high-speed application is important, as it makes the natural frequency speed-dependent with forward and backward natural frequencies. The forward and backward frequencies are identical at zero shaft speed. However, as the speed increases, the vibration starts to show two whirl natural frequencies: the forward and backward natural frequencies; the higher the gyroscopic effect, the more difference between the forward and backward components. For the forward natural frequencies, the gyroscopic effect shows a stiffening effect, which raises the forward whirl frequency. For the backward natural frequencies, the gyroscopic effect contributes positive kinetic energy and tends to lower the corresponding backward whirl frequency [5]. When the system damping is low, two closely spaced critical speeds could be observed. Operating between the two critical speeds can make the machine sensitive to rotor-stator rubbing since the rotor may be executing line-to-line or backward whirl under such conditions [6].

Greenhill and Cornejo [7] reported that the direct stiffness asymmetry has a significant influence on the backward whirl natural frequency excitation. When the speed is high, asynchronous (forward/backward) whirl motion may occur due to the fluid film bearing anisotropic properties. Such asynchronous whirl motion may occur even in the perfectly balanced rotor due to momentarily transverse disturbances [8]. Besides, labyrinth seal cross-coupling forces could significantly reduce the damping ratio of the forward natural frequency. Thus, identifying the forward natural frequencies from backward natural frequencies is necessary for the compressor design and test. When diagnosing subsynchronous vibrations, it is important to note the whirl direction (forward/backward), which helps distinguish oil whirl and whip from shaft rub and other anomalies that produce backward procession [6].

Traditional full spectrum plots and orbits process data from two orthogonal transducers can provide information on the ellipticity of the orbit and direction of vibration [9-11]. It is easy to determine the ellipticity and direction of the orbit with the amplitude relationship between forward and backward vibration components of a full spectrum. It is an engineering practice to identify the compressor forward and backward natural frequencies via the excitation test using a magnetic bearing. The magnetic bearings allow users to control the amplitudes and phase angles of the forces applied along with the horizontal and vertical directions. The magnetic bearing generates a rotating force with the same direction as the rotor's spinning motion to excite the forward natural frequencies. Similarly, applying a rotating force against the rotor rotating direction could excite the backward natural frequencies.

Cloud et al. [12] found that the use of the single degree of freedom (SDOF) techniques to identify the system amplification factor (AF) and log decrement may yield unreliable results. The close proximity of forward and backward whirling components is the primary cause. To identify the forward and backward components, prior researchers have introduced different methods both theoretically and experimentally. Childs [13] presented a theoretical solution to identify the forward and backward components. The solutions to the elliptical orbits of a rotor response are in the complex variable form, where the complex coefficients are the associated forward and backward amplitudes. Cloud and Kocur [14] compared the experimental methods to separate the forward and backward components. For time-domain response measurements, processing the test results with the multiple output backward autoregression method; and the prediction error method (PEM) for frequency response function (FRF) measurements. In 2010, Pettinato et al. [15] identified the forward and backward natural frequencies with magnetic bearing exciter excitations. At each operating point, the test includes two sets of single input multiple output (SIMO) FRFs over a frequency range from 30 Hz to 170 Hz. For each operating point, it took approximately 30 minutes to complete the sinusoidal testing. In 2012, based on the modal testing theory proposed by Lee [16], Takahashi et al. [17] evaluated a centrifugal compressor with the electromagnetic exciter. Takahashi et al. [17] obtained a directional frequency response function (dFRF) from four frequency response functions. By using a complex number expression for the rotor motion, they separated the forward and backward natural frequencies in frequency domain. This paper presents an effective method to separate the forward and backward natural frequencies simultaneously from a planar excitation response. The full load full pressure shop test of a 21,700 HP (16 MW) centrifugal compressor serves to validate the method. For each operating speed, the total excitation test time is less than 3 minutes.

METHOD TO SEPARATE FORWARD AND BACKWARD ORBITS

During operation, proximity transducers mounted on the machine measure the relative distances between the rotor and transducers. The rotor center orbit plot demonstrates the manner in which the rotor vibrates during the operation through relative distances, as illustrated in Figure 1. The rotor orbit can be expanded into a sum of filtered orbits with frequencies correspond to 1× (synchronous speed), 2×… synchronous speed, see Figure 2.

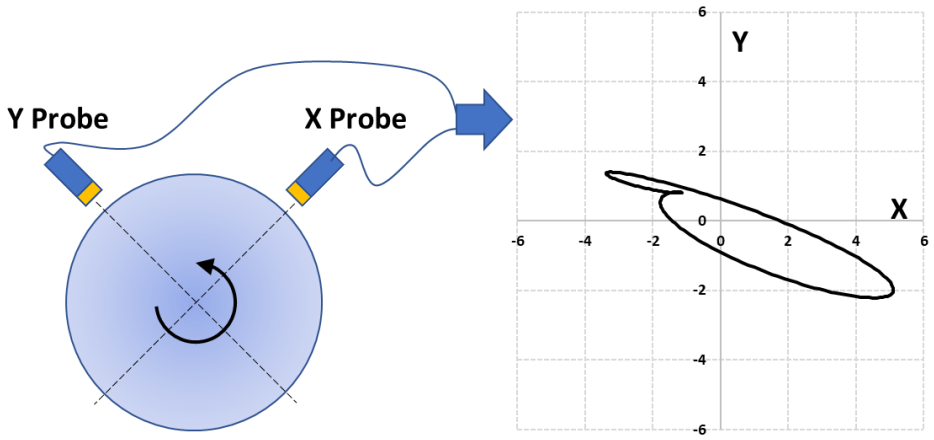

Figure 1. Typical proximity transducer signal

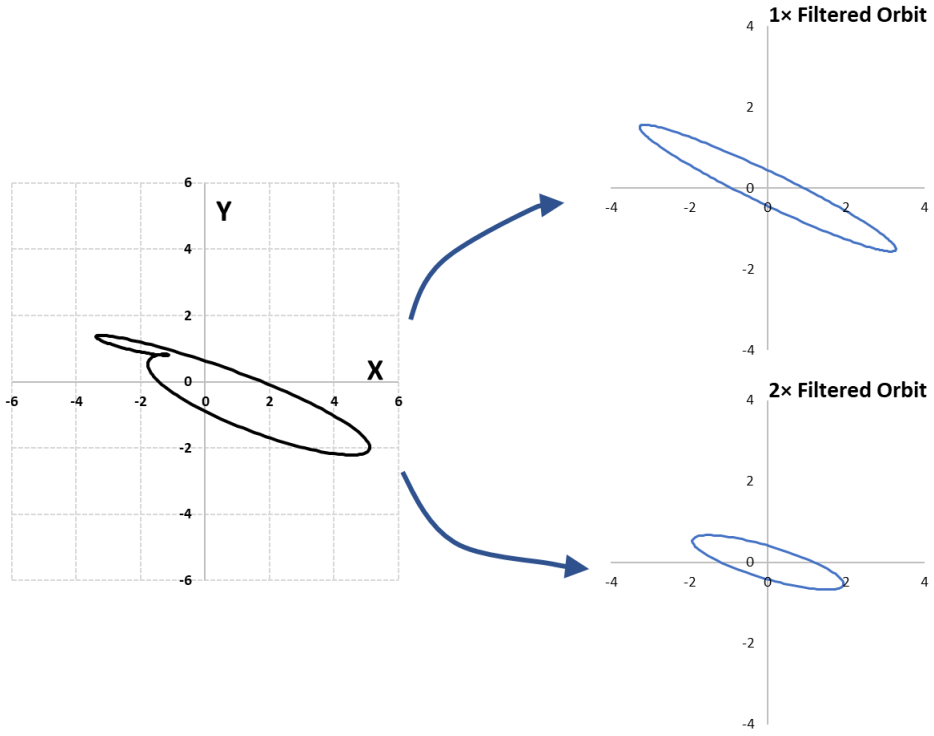

Figure 2. Expansion of the direct orbit

In general, each filtered orbit has an elliptical shape, and the elliptical orbit can be presented as a sum of two circular orbits that rotate at the filtered orbit frequency: one rotates in the same direction as the rotor (forward), and the other is in the opposite direction (backward). Figure 3(a) demonstrates the decomposition of the 1× filtered orbit. As discussed in Ref. [11], the filtered orbit could be expressed in two parts consisting of the forward (*FW*) motion and the backward (*BW*) motion. When the forward motion is dominant (has a larger amplitude than the *BW* motion), the filtered orbit moves along the same direction as rotor rotation. Similarly, the filtered orbit moves against the rotor rotation direction when the backward motion is dominant. If the filtered orbit is circular and forward, see Figure 3(b), then the backward motion does not exist. On the other hand, as shown in Figure 3(c), if the filtered orbit is a straight line, then the forward and backward motions have equal amplitudes. The relative phase angle determines the orientation of the filtered orbit.

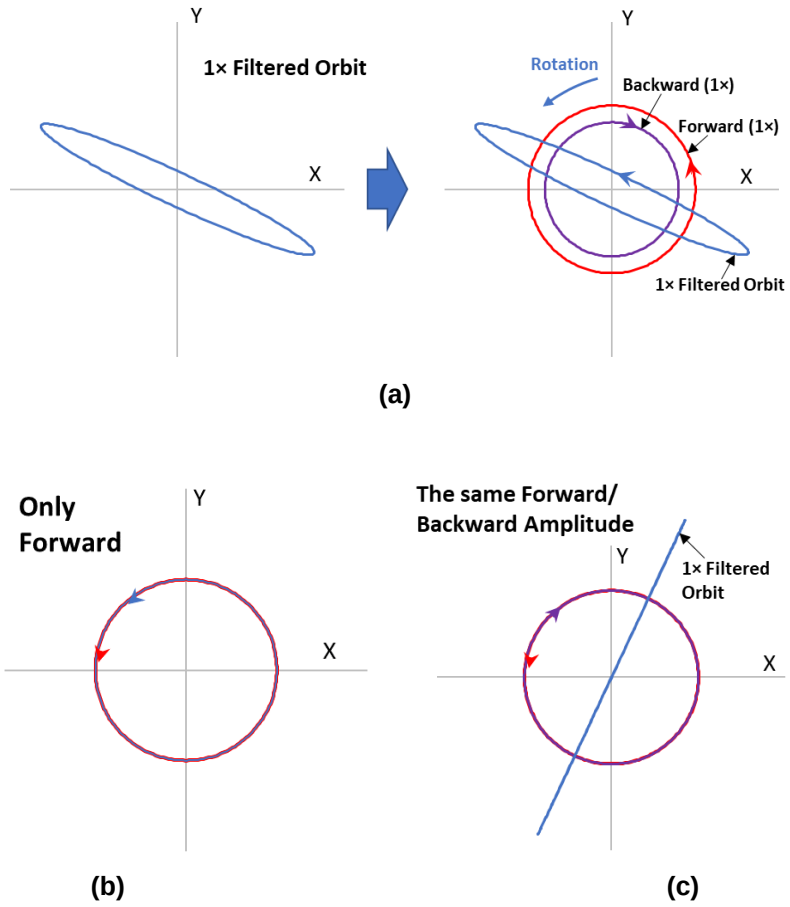

Figure 3. The filtered orbit characteristic with respect to the forward/backward motions.

In general, at any given time, the f*iltered orbit = FW+ BW*, see Figure 4. Both the forward and backward motions have the same frequency ω as the filtered orbit, while different amplitudes and phase angles. That is,

$$\text{For the filtered orbit: } \begin{cases} X = X_{FW} + X_{BW} \\ Y = Y_{FW} + Y_{BW} \end{cases} \tag{1}$$

$$\text{For the Forward motion } \begin{cases} X_{FW} = R_{FW}\cos(\omega t + \alpha) \\ Y_{FW} = R_{FW}\sin(\omega t + \alpha) \end{cases} \tag{2}$$

where R_{FW} is the forward amplitude, and α is the forward phase angle.

$$\text{For the Backward motion } \begin{cases} X_{BW} = R_{BW}\cos(-\omega t + \beta) \\ Y_{BW} = R_{BW}\sin(-\omega t + \beta) \end{cases} \tag{3}$$

where R_{BW} is the backward amplitude, and β is the backward phase angle.

Therefore, the filtered orbit could be expressed as:

$$\rightarrow \begin{cases} X = X_{FW} + X_{BW} = R_{FW}\cos(\omega t + \alpha) + R_{BW}\cos(-\omega t + \beta) \\ Y = Y_{FW} + Y_{BW} = R_{FW}\sin(\omega t + \alpha) + R_{BW}\sin(-\omega t + \beta) \end{cases} \quad (4)$$

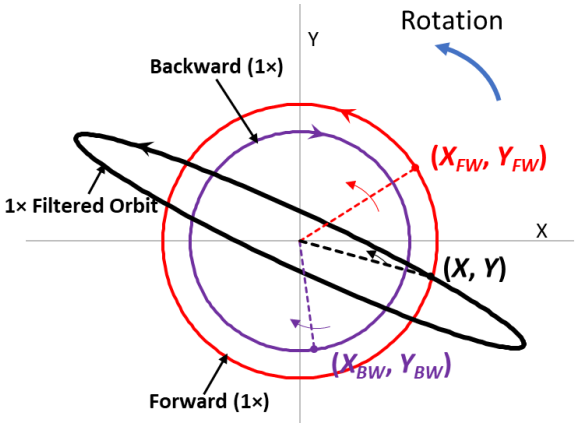

Figure 4. Relation between the filtered orbit and forward and backward motions.

Figure 5 depicts the peak-peak values of the filtered orbit. At these points with maximum X or Y coordinates, the amplitude $|X_{Max}|$ and $|Y_{Max}|$ equal ½ of the peak-peak values ($X_{P\text{-}P}$ and $Y_{P\text{-}P}$), respectively. During a test, the data acquisition system (e.g., ADRE) outputs the peak-peak amplitude values at the filtered frequency (1×, 2×, …), i.e., $(X_{P-P}, \text{Phase}_{@X_{Peak}})$ and $(Y_{P-P}, \text{Phase}_{@Y_{Peak}})$.

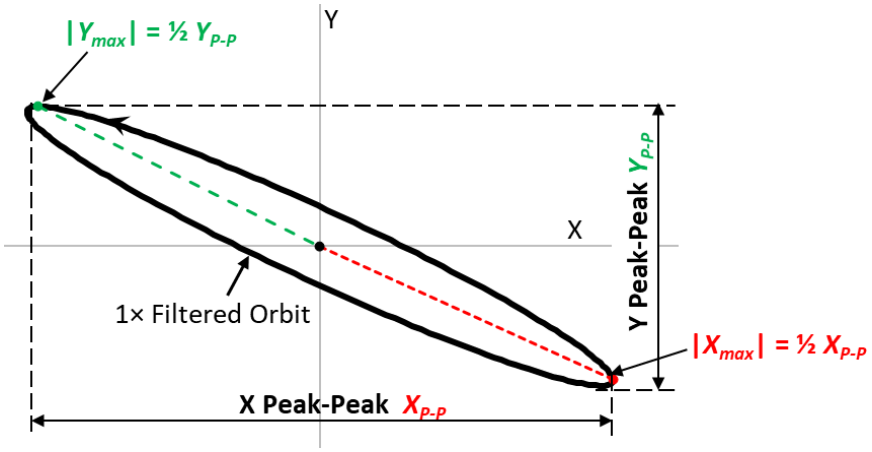

Figure 5. Peak values of the filtered orbit.

Recall Eqn. (4), at the X and Y direction peak values, we have

$$X_{Max} = X_{FW} + X_{BW} = R_{FW}\cos(\omega t_1 + \alpha) + R_{BW}\cos(-\omega t_1 + \beta) \quad (5)$$

$$Y_{Max} = Y_{FW} + Y_{BW} = R_{FW}\sin(\omega t_2 + \alpha) + R_{BW}\sin(-\omega t_2 + \beta) \quad (6)$$

There are four unknowns in the above equations: R_{FW}, R_{BW}, α, and β. To identify the forward and backward whirl components, two additional independent equations are required. When the orbit reaches the X direction maximum value (X_{Max}), the first time derivative of X, dX/dt, reaches zero. Then

$$\frac{dX_{Max}}{dt} = -R_{FW}\omega\sin(\omega t_1 + \alpha) + R_{BW}\omega\sin(-\omega t_1 + \beta) = 0 \quad (7)$$

Similarly, for the Y_{Max} location,

$$\frac{dY_{Max}}{dt} = R_{FW}\omega\cos(\omega t_2 + \alpha) - R_{BW}\omega\cos(-\omega t_2 + \beta) = 0 \tag{8}$$

Thus, from the filtered orbit, we have four independent equations:

$$\begin{cases} X_{Max} = X_{FW} + X_{BW} = R_{FW}\cos(\omega t_1 + \alpha) + R_{BW}\cos(-\omega t_1 + \beta) \\ Y_{Max} = Y_{FW} + Y_{BW} = R_{FW}\sin(\omega t_2 + \alpha) + R_{BW}\sin(-\omega t_2 + \beta) \\ 0 = -R_{FW}\omega\sin(\omega t_1 + \alpha) + R_{BW}\omega\sin(-\omega t_1 + \beta) \\ 0 = R_{FW}\omega\cos(\omega t_2 + \alpha) - R_{BW}\omega\cos(-\omega t_2 + \beta) \end{cases} \tag{9}$$

Figure 6(a) depicts a rotor orbit (1× filtered at a frequency ω = 1,372 CPM) of a production compressor tested by the authors' company. The tabulated results give peak-peak amplitudes (X_{Max} = 0.881 mil, Y_{Max}= 0.808 mil) and associated phase angles ($\text{Phase}_{@X_{Peak}}$, $\text{Phase}_{@Y_{Peak}}$) along X and Y directions. Substituting these parameters into the Eqn. (9),

$$\begin{cases} X_{Max} = R_{FW}\cos\left(\text{Phase}_{@X_{Peak}} + \bar{\alpha}\right) + R_{BW}\cos\left(-\text{Phase}_{@X_{Peak}} + \bar{\beta}\right) \\ Y_{Max} = R_{FW}\sin\left(\text{Phase}_{@Y_{Peak}} + \bar{\alpha}\right) + R_{BW}\sin\left(-\text{Phase}_{@Y_{Peak}} + \bar{\beta}\right) \\ 0 = -R_{FW}\omega\sin\left(\text{Phase}_{@X_{Peak}} + \bar{\alpha}\right) + R_{BW}\omega\sin\left(-\text{Phase}_{@X_{Peak}} + \bar{\beta}\right) \\ 0 = R_{FW}\omega\cos\left(\text{Phase}_{@Y_{Peak}} + \bar{\alpha}\right) - R_{BW}\omega\cos\left(-\text{Phase}_{@Y_{Peak}} + \bar{\beta}\right) \end{cases} \tag{10}$$

where, $\bar{\alpha}$ and $\bar{\beta}$ are the forward and backward natural frequencies phase angles relative to the filtered orbit. Figure 6(b) illustrates the calculated rotor forward and backward orbits through Eqn. (10). Superimposing the calculated forward and backward orbits, the predicted rotor orbit (blue dashed line) shows a good agreement with the measurement.

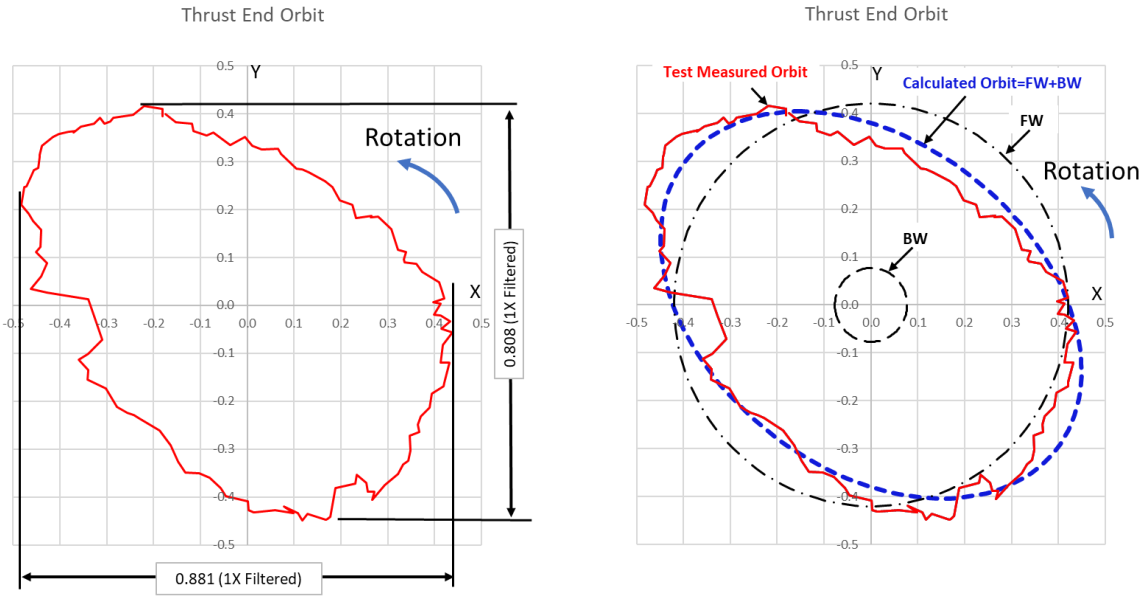

(a) **(b)**

Figure 6. Filtered (1×) orbit of a contract compressor rotor: (a) the measured rotor orbit (1× filtered); (b) comparison between the calculated and measured rotor orbit (1× filtered)

CRITICAL SPEEDS IDENTIFICATION USING PROPOSED METHOD

CASE #1

This example identifies the first forward and backward critical speeds of a multistage centrifugal compressor. To verify the method, the authors conducted harmonic excitation analysis for the rotor illustrated in Figure 7. Please note that the selection of operating speed in the analysis may change the critical speed location due to the bearing coefficients speed dependent characteristics. Prior test results indicate that the compressor's first forward and backward natural frequencies are close to each other and difficult to be directly identified through the test or numerical analysis. However, applying the same excitation along with both *X* and *Y* directions, namely, planar excitation, the rotor response includes forward and backward natural frequency responses.

Figure 8 shows the Bode plot of the compressor's planar excitation (45 degree at the mid-span) response, which contains both the forward and backward responses. The backward/forward critical speeds are expected to be within the range of 4,996 CPM to 5,088 CPM. Solving equation 10 at each frequency point gives the forward and backward amplitudes at each frequency point. Figure 9 plots the calculated amplitudes and phase angles versus the excitation frequency for both forward and backward natural frequencies. Based on the planar excitation response, the calculated backward natural frequency is 5,034 CPM, and the forward natural frequency is 5,146 CPM. Please note that the phase angle plots in Figure 9 are for the relative phase angles, not the actual phase angle.

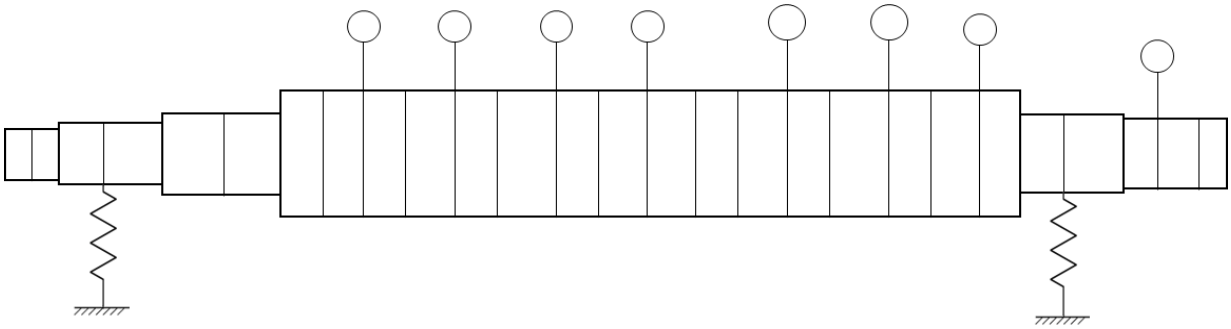

Figure 7. A typical centrifugal compressor model (not to scale).

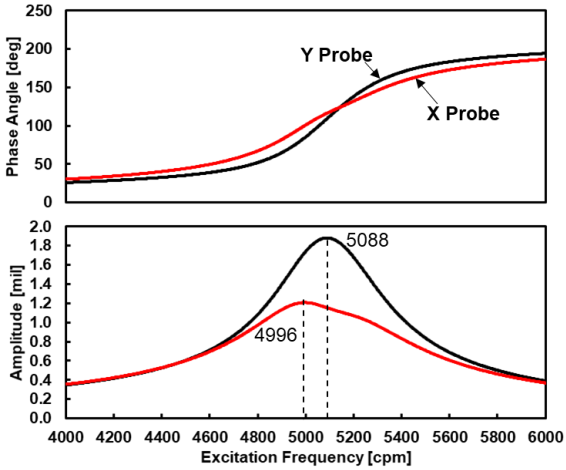

Figure 8. Compressor planar excitation response.

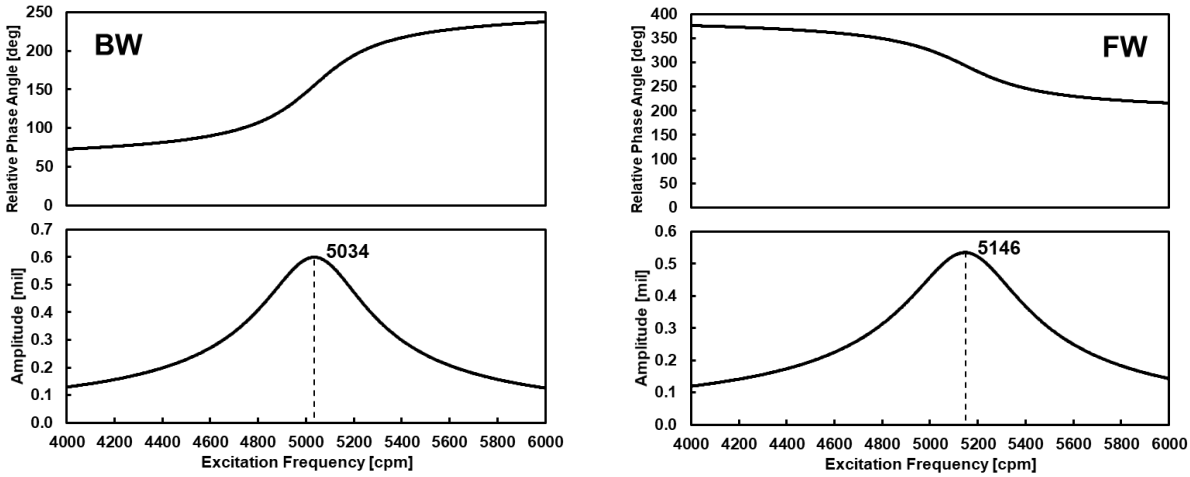

Figure 9. Separated backward and forward responses vs. excitation frequency: (a) Backward; (b) Forward.

As discussed earlier, applying an excitation with/against the rotor rotating direction excites the forward/backward natural frequency response, and we can readily identify the forward critical speed. To verify the calculation results, the authors conducted harmonic excitation analysis with backward and forward excitations, respectively. Figure 10 shows the backward/forward excitation responses, which gives the backward natural frequency is 5,038 CPM, and the forward natural frequency is 5,142 CPM. The rotating excitation response results confirm that this method can effectively separate the forward and backward natural frequencies from the planar excitation response; alas, the two natural frequencies are very close to each other (in this case, the forward critical speed is 2% higher than the backward).

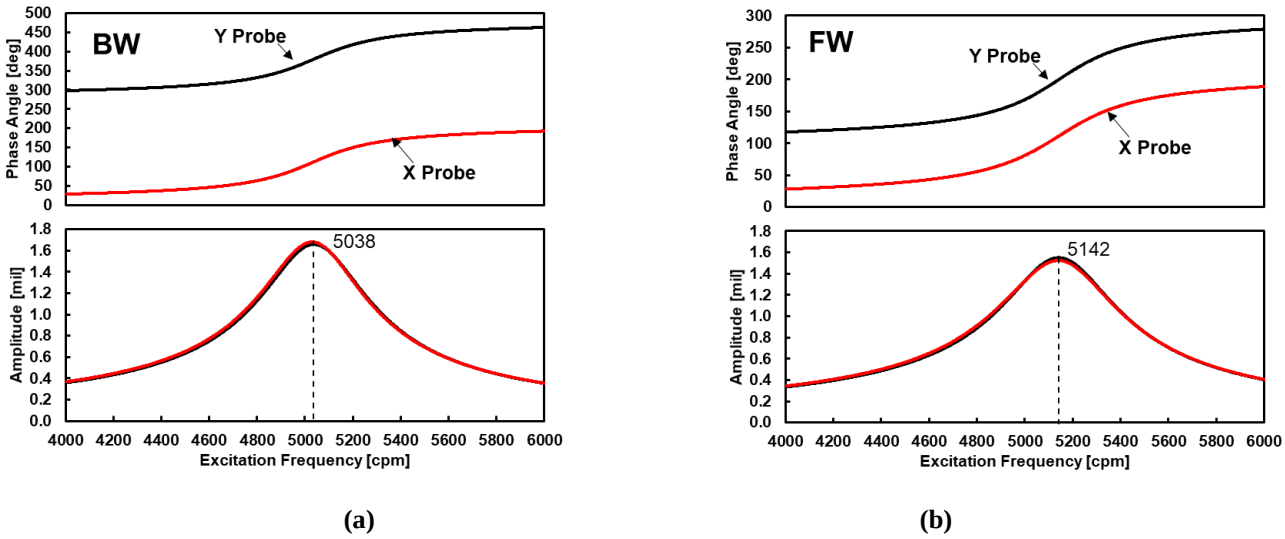

Figure 10. Compressor harmonic excitation responses with rotating force: (a) backward excitation and (b) forward excitation.

CASE #2

Recently, the authors' company tested a 6 stage back-to-back centrifugal compressor (16 MW) designed for natural gas processing. The main focus is the identification and extraction of the first and second forward and backward natural frequencies from the measured results of the full-load, full-pressure test with a magnetitic bearing exciter. Figure 11 shows a damped Eigenvalue Plot which identifies the damped natural frequencies of the rotor system. The natural frequencies are determined from the intersection of the inclined

synchronous excitation line with the roughly horizontal natural frequency curves. For this rotor, the first backward natural frequency is approximately 6,129 CPM, and approximately 6,487 CPM for the first forward natural frequency. The predicted second backward and forward natural frequencies locate at 21,533 CPM and 22,980 CPM, respectively. Figure 12 illustrates the test apparatus with a magnetic bearing exciter (MBE) for identifying the compressor's natural frequencies. As depicted in the schematic plot, the MBE generates the same forces (amplitude and phase) applied along with the horizontal and vertical directions, resulting in a planar excitation on the rotor. As the numerical analysis indicates the compressor's first natural frequency is around 6,250 CPM; thus, a frequency sweep from 80 Hz (4,800 CPM) to 150 Hz (9,000 CPM) with 1 Hz resolution is sufficient to capture the critical speed.

Figure 13 displays the planar excitation response with the above frequency sweep. The authors conducted a least square curve fit of the data, where the symbols represent measured data, and the lines stand for the curve-fitted data as shown in Figure 14. Figure 15 depicts the separated forward and backward natural frequencies, and the corresponding natural frequencies are 6,350 CPM and 6,500 CPM, respectively. The discrepancies between the predicted and measured first forward/backward natural frequencies are less than 3.5%.

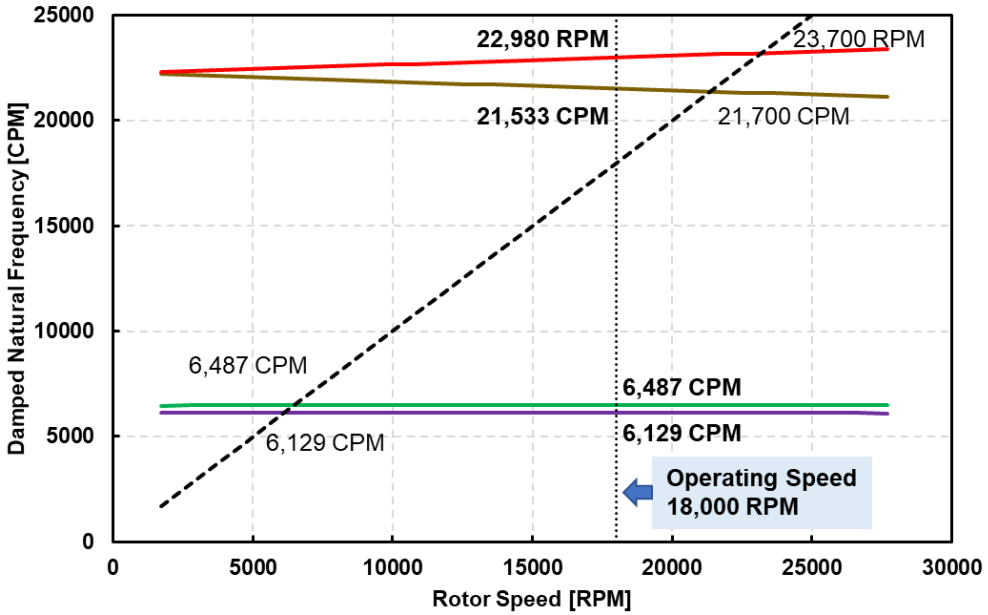

Figure 11. Predicted damped natural frequency.

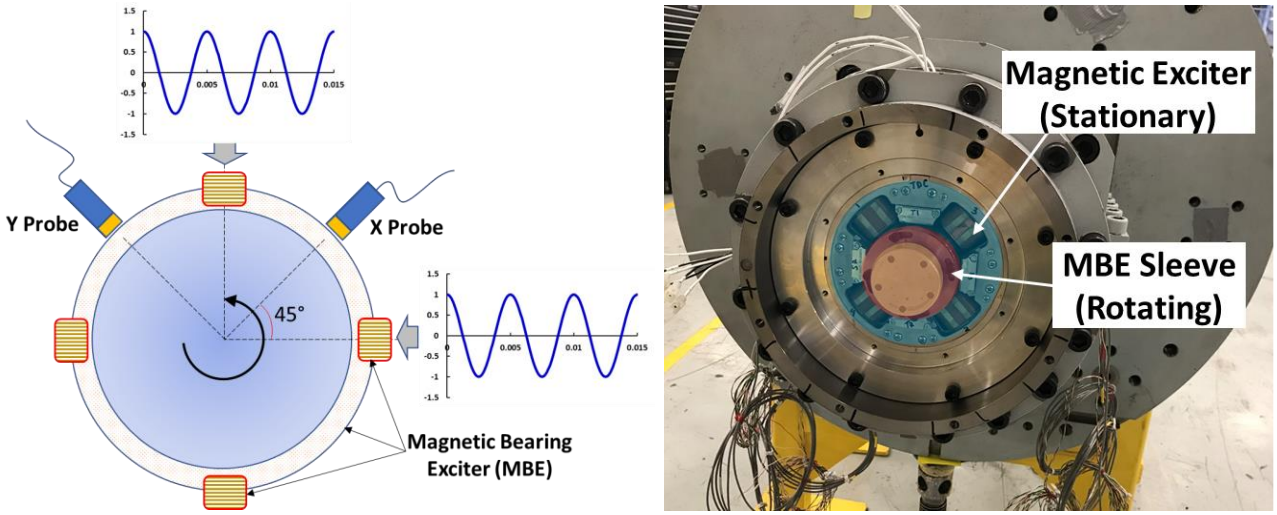

(a) schematic view **(b) Test Apparatus**

Figure 12. Test apparatus with magnetic bearing exciter.

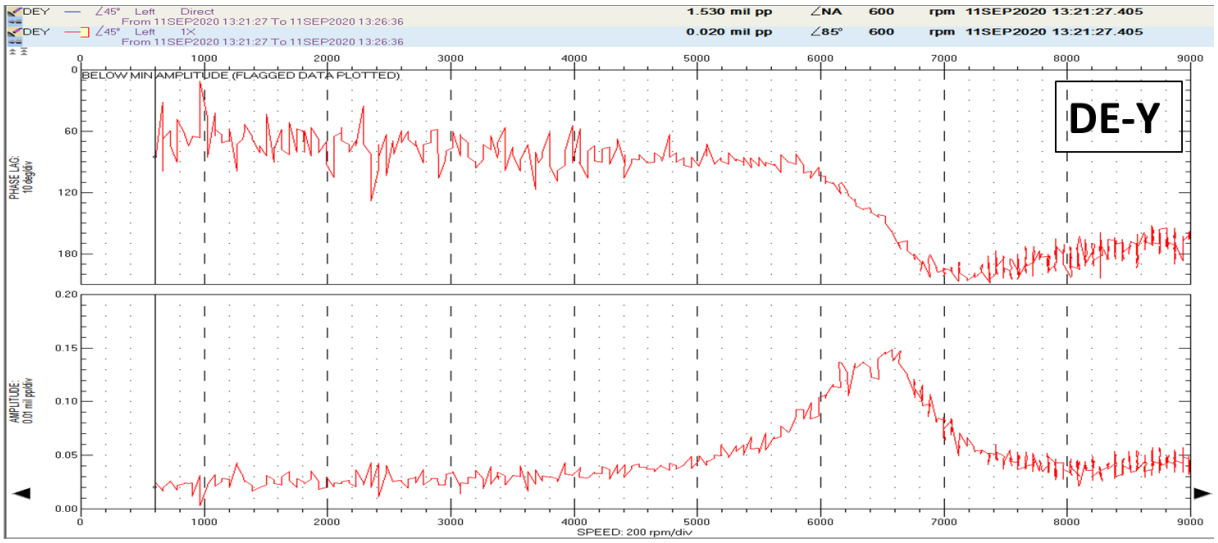

Figure 13. Test measured planar excitation response around first bending critical speed (running speed at 18,000 RPM).

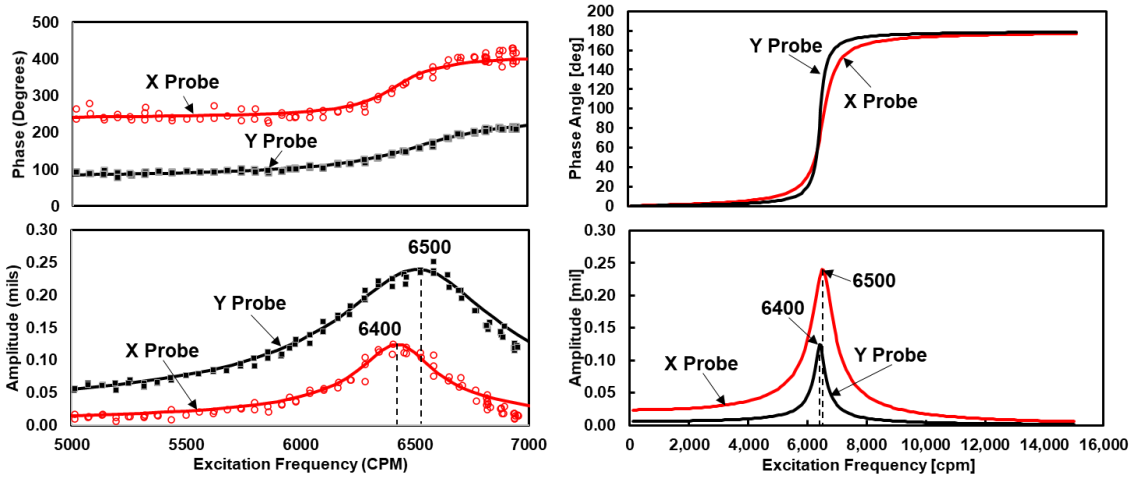

(a) **(b)**

Figure 14. Test measured planar excitation response for the first critical speed: (a) measured data (5,000 – 7,000 CPM); (b) curve fit data (0 – 15,000 CPM).

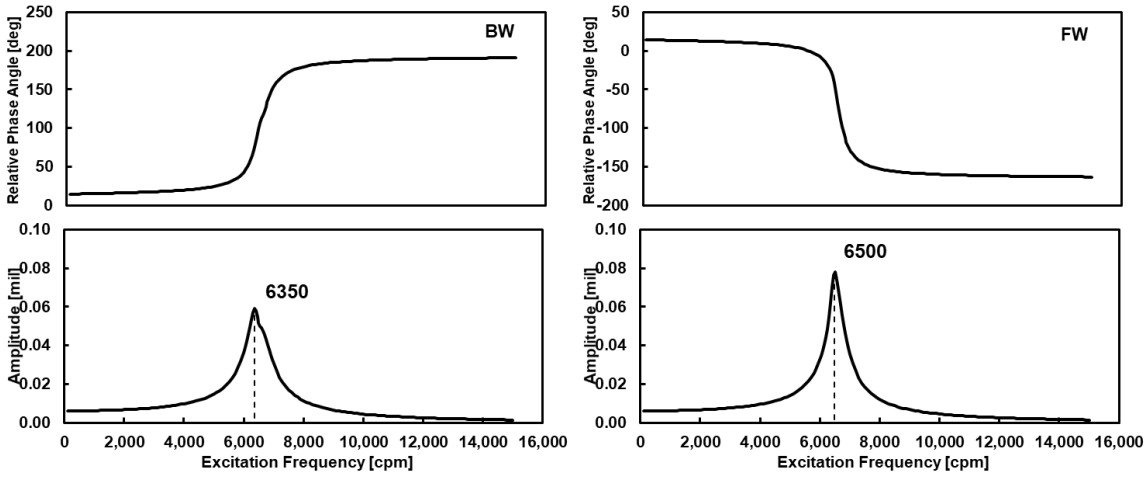

(a) **(b)**

Figure 15. Separated first forward and backward natural frequencies for the measured planar excitation response (around the 1st bending mode).

A frequency sweep from 315 HZ (19,000 CPM) to 417 Hz (25,000 CPM) with 1 Hz resolution is applied to capture the second natural frequency.

Figure 16 displays the planar excitation response with the above frequency sweep. Due to the gyroscopic effect, the response plot has two distinct peaks at 21,620 CPM and 23,670 CPM. Please note that the response is a superposition of the forward and backward natural frequencies. Thus, the peaks are not the actual forward/backward natural frequencies. Applying the proposed separation method in this paper, Figure 17 shows the separated backward and forward responses, and the corresponding natural frequencies are 21,845 CPM and 23,540 CPM, respectively. Thus, the superposition of the forward and backward responses shifts the backward and forward peaks slightly. The backward natural frequency directly identified from the planar excitation response plot is slightly lower (1.6%) than its predicted value. Similarly, the predicted forward natural frequency is slightly lower than its value identified directly from the planar excitation response plot. The predicted second bending natural frequencies agree with the measured results within 2.4%.

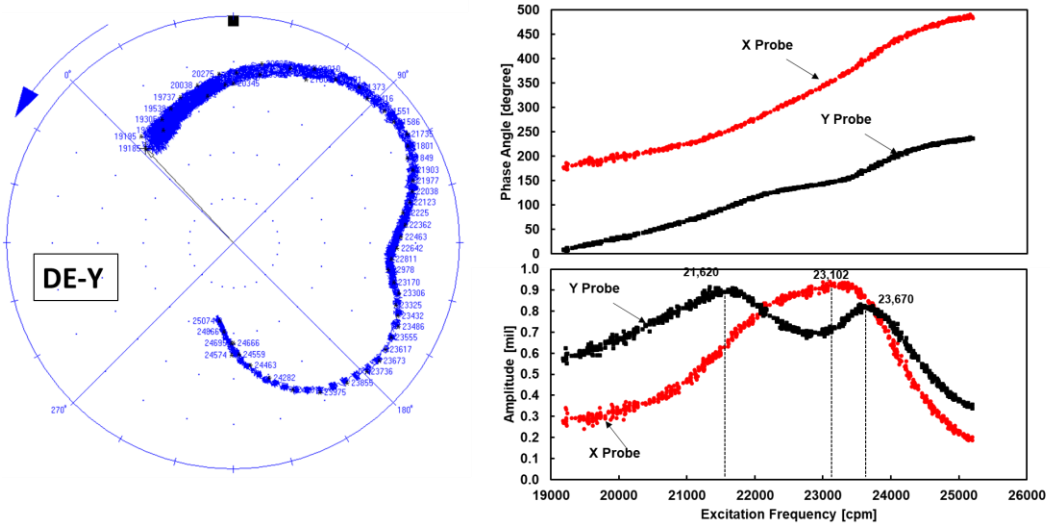

(a) rotor orbit on drive end

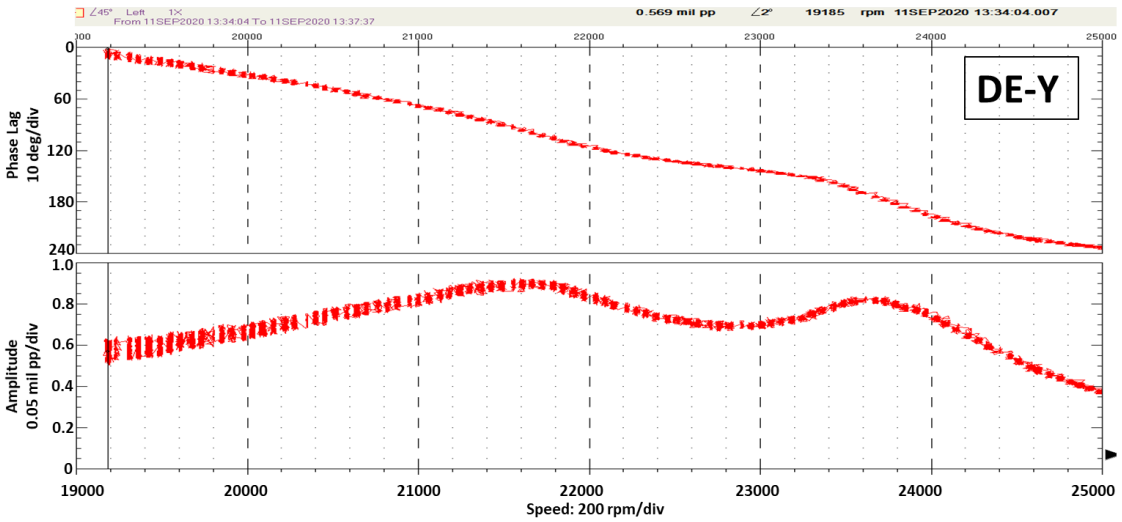

(b) drive end vertical direction

Figure 16. Test measured planar excitation response around the 2nd bending critical speed (running speed at 18,000 RPM).

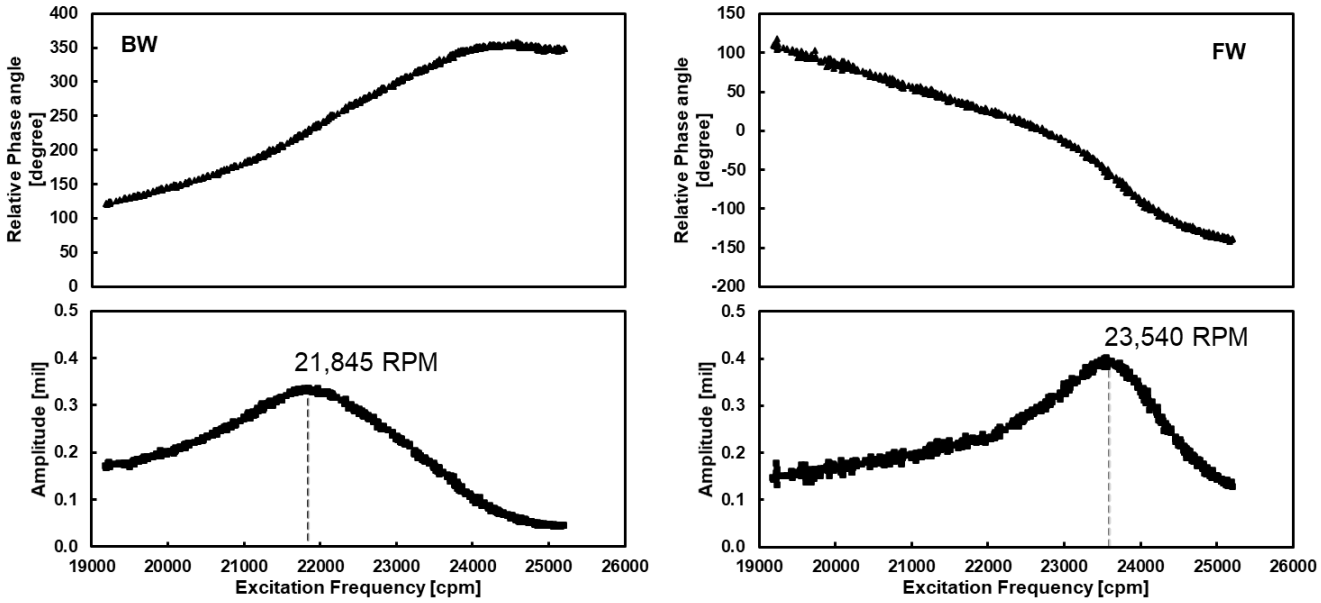

(a) **(b)**

Figure 17. Separated second forward and backward natural frequencies for the measured planar excitation response (around the 2nd bending mode).

CONCLUSION

In the prior engineering practice, a rotor is excited with rotating forces with and against the rotor rotating direction to identify the compressor's forward and backward natural frequencies, respectively. This paper demonstrates an effective approach to identify the forward and backward natural frequencies from a single planar excitation. The first case study shows that the proposed method effectively separates the forward and backward natural frequencies though the two natural frequencies are close to each other (the forward critical speed is only 2% higher than the backward). In the second case study, the authors' company conducted a full pressure full load test of a 16 MW compressor. With the magnetic bearing exciter (MBE), excitations at both sub-synchronous and super-

synchronous frequency ranges are applied on the rotor to obtain the first and second critical speeds. By applying the proposed method, the forward and backward natural frequencies are effectively identified.

Furthermore, to identify the rotor backward and forward natural frequencies without a magnetic bearing exciter (MBE), two mechanical shakers are required at X and Y directions to generate the backward and forward rotating forces. With the proposed method, only one shaker at arbitrary direction is sufficient. On the other hand, in machinery vibration problems diagnosis, this paper's method enables engineers to readily separate the backward vibration component from the field test data. Thus, helping the engineers better conduct root cause analyses.

NOMENCLATURE

α, β	= Phase Angle [deg]
$\bar{\alpha}, \bar{\beta}$	= Relative Phase Angle [deg]
BW	= Backward
FW	= Forward
MBE	= Magnetic Bearing Exciter
MCOS	= Maximum Continuous Operating Speed
R_{BW}, R_{BW}	= Forward/Backward Amplitude [m]
t	= Time [s]
ω	= Excitation Frequency [Hz]
Ω	= Rotor Speed [RPM]
X, Y	= X/Y direction
$X_{P\text{-}P}$, $Y_{P\text{-}P}$	= Peak-Peak Amplitude along X, Y direction [m]
X_{Max}, Y_{Max}	= Maximum Amplitude along X, Y direction [m]

REFERENCES

[1] American Petroleum Institute, 2014, "API 617 Standard 8th Edition: Axial and Centrifugal Compressors and Expander-Compressors".

[2] Cloud, C. H., "Design Audits of Machinery–Rotor Dynamics," Proc. The Twenty-First Ethylene Producers' Conference.

[3] Atkins, K., Perez, R., PE Sr, R. E., Refining, C., and Turner, D., "A Simple Procedure for Assessing Rotor Stability," Proc. Rotating machinery--transport phenomena: proceedings of the Third International Symposium on Transport Phenomena and Dynamics of Rotating Machinery (ISROMAC-3), CRC Press, p. 361

[4] Atkins, K. E., Tison, J. D., and Wachel, J., "Critical Speed Analysis of an Eight-Stage Centrifugal Pump," Proc. Proceedings of the 2nd International Pump Symposium, Turbomachinery Laboratories, Department of Mechanical Engineering, Texas A&M …,

[5] Chen, W. J., 2015, Practical Rotordynamics and Fluid Film Bearing Design, Trafford On Demand Pub, Davidson, NC.

[6] Vance, J. M., Murphy, B., and Zeidan, F., 2010, "Machinery Vibration and Rotordynamics," Wiley, Hoboken, N.J.

[7] Greenhill, L. M., and Cornejo, G. A., 1995, "Critical Speeds Resulting from Unbalance Excitation of Backward Whirl Modes," Design Engineering Technical Conferences, **3**(part 3-B), pp. 991-1000

[8] Tiwari, R., 2017, Rotor Systems: Analysis and Identification, CRC Press, Boca Raton.

[9] Southwick, D., 1993, "Using Full Spectrum Plots," Orbit, **14**(4)

[10] Southwick, D., 1994, "Using Full Spectrum Plots Part 2," Orbit, **15**(2)

[11] Goldman, P., and Muszynska, A., 1999, "Application of Full Spectrum to Rotating Machinery Diagnostics," Orbit, **20**(1), pp. 17-21.

[12] Cloud, C. H., Maslen, E. H., and Barrett, L. E., 2009, "Damping Ratio Estimation Techniques for Rotordynamic Stability Measurements,"

[13] Childs, D., 1993, Turbomachinery Rotordynamics-Phenomena, Modeling and Analysis-Dara W. Childs, John Wiley & Sons

[14] Cloud, C. H., and Kocur, J., "Shop Rotordynamic Testing-Options, Objectives, Benefits & Practices," Proc. Asia Turbomachinery & Pump Symposium. 2016 Proceedings., Turbomachinery Laboratories, Texas A&M Engineering Experiment Station,

[15] Pettinato, B. C., Cloud, C. H., and Campos, R. S., 2010, "Shop Acceptance Testing of Compressor Rotordynamic Stability and Theoretical Correlation," Proc. Proceedings of the 39th Turbomachinery Symposium, Texas A&M University. Turbomachinery Laboratories,

[16] Lee, C.-W., 1991, "A Complex Modal Testing Theory for Rotating Machinery," Mechanical Systems and Signal Processing, **5**(2), pp. 119-137

[17] Takahashi, N., Magara, Y., Narita, M., and Miura, H., 2012, "Rotordynamic Evaluation of Centrifugal Compressor Using Electromagnetic Exciter," Journal of Engineering for Gas Turbines and Power, **134**(3), doi:10.1115/1.4004439.